

Multi-scale Unified Network for Image Classification

Wenzhuo Liu, Fei Zhu, Cheng-Lin Liu *Fellow, IEEE*

Abstract—Convolutional Neural Networks (CNNs) have advanced significantly in visual representation learning and recognition. However, they face notable challenges in performance and computational efficiency when dealing with real-world, multi-scale image inputs. Conventional methods rescale all input images into a fixed size, wherein a larger fixed size favors performance but rescaling small size images to a larger size incurs digitization noise and increased computation cost. In this work, we carry out a comprehensive, layer-wise investigation of CNN models in response to scale variation, based on Centered Kernel Alignment (CKA) analysis. The observations reveal that lower layers are more sensitive to input image scale variations than high-level layers. Inspired by this insight, we propose Multi-scale Unified Network (MUSN) consisting of multi-scale subnets, a unified network, and scale-invariant constraint. Our method divides the shallow layers into multi-scale subnets to enable feature extraction from multi-scale inputs, and the low-level features are unified in deep layers for extracting high-level semantic features. A scale-invariant constraint is posed to maintain feature consistency across different scales. Extensive experiments on ImageNet and other scale-diverse datasets, demonstrate that MSUN achieves significant improvements in both model performance and computational efficiency. Particularly, MSUN yields an accuracy increase up to 44.53% and diminishes FLOPs by 7.01-16.13% in multi-scale scenarios.

Index Terms—Image Classification, Convolutional Neural Networks, Scale-invariant, Multi-scale Unified Network

I. INTRODUCTION

Convolutional neural networks (CNNs) have become the dominant approach for visual representation learning, achieving state-of-the-art performance in various tasks [42], [58], [73]. CNNs have proven highly effective in capturing hierarchical features and learning complex patterns in visual data through training on large datasets [10], [69], [74]. However, despite their remarkable success, CNNs still face performance and computational efficiency challenges when handling inputs of different scales [25], [26], [59], [66].

For convenience of processing by neural networks, the input image is often scaled to a uniform size, such as the widely used 224×224 size for ImageNet [30]. This practice can be traced back to the pioneering AlexNet, which utilized a consistent input size in the ImageNet classification competition, followed by subsequent architectures like VGGNet [50] and ResNet [22]. Resizing input images is helpful for improving training efficiency, such as mini-batch learning through gradient

The authors are with the School of Artificial Intelligence, University of Chinese Academy of Sciences, Beijing 100049, P.R. China, and the State Key Laboratory of Multimodal Artificial Intelligence Systems, Institute of Automation of Chinese Academy of Sciences, 95 Zhongguancun East Road, Beijing 100190, P.R. China.

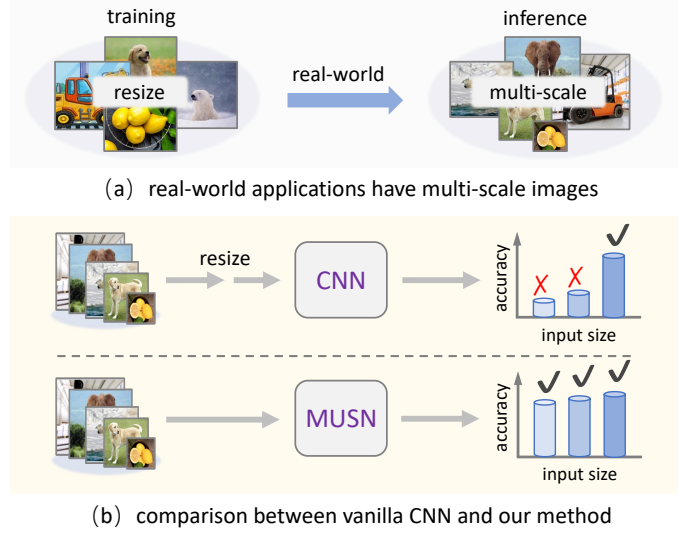


Fig. 1. In the real world, images come in different sizes, but Vanilla models are designed for a fixed input size, causing performance degradation when the input image scale changes. In contrast, MSUN retains stable performance over a range of scales.

descent, which necessitates the same input size for all images in a batch for efficient parallel training of CNNs [1].

However, uniform input size conflicts with real-world scenarios, where images are naturally in variable scales¹, due to the variations of camera devices/parameters, object scale and imaging distance. This discrepancy can severely impact a trained CNN's performance and computational efficiency when applied to different image sizes [2], [19], [47]. For instance, in our experiments, when testing a ResNet50 model trained on ImageNet resizing images from 224×224 to 32×32 , the accuracy drops from 75.18% to 19.64%. Moreover, to adapt to the model's input size, upsampling a 32×32 image to 224×224 would increase the computational cost by 250.54%.

A layer-by-layer analysis of CNN models is crucial to address the challenges of performance degradation and computational complexity when handling multi-scale input images. LeCun et al. [31] and Goodfellow et al. [21] have provided comprehensive overviews of hierarchical feature extraction capabilities. It is widely recognized that shallow layers capture low-level features such as edges and textures, while deeper layers extract complex, high-level semantic information. In this work, we analyze the layerwise impacts of CNN models on multi-scale inputs, using Centered Kernel Alignment (CKA) metric [15], [27] to evaluate feature similarity across layers.

¹The term *scale* has many different meanings according to the different factors in imaging. In this paper, we refer *scale* specially to the size of image input to neural networks.

In analyzing many CNN models like ResNet, DenseNet, VGGNet, and MobileNet, we observe a common phenomenon that *lower layers exhibit more pronounced sensitivity to scale variations*. As image scales change, the substantial alterations in features extracted by these lower layers result in degraded accuracy.

These insights lead us to redesign CNNs to enhance the adaptability of models under multi-scale input images. The primary idea is to separate shallow layers for extracting features at different scales, as they are more sensitive to scale changes. Specifically, distinct lower layers are used to extract features from inputs of different scales, so as to ameliorate the sensitivity to input scale. We then implement scale-invariant constraint to maintain consistency in the features across different scales, an approach commonly applied in traditional handcrafted features such as SIFT [36] and SURF [4]. After that, a unified network is used to learn high-level semantic information in the higher layers. We refer to this model as Multi-scale Unified Network (MSUN).

Our method can be directly applied to various CNN architectures, significantly enhancing the adaptability in multi-scale scenarios without complicated modifications and increased computational costs. It improves the recognition performance in numerous experiments, including evaluations on ImageNet with varying scales and transfer learning on CIFAR-100 [29], STL-10 [14], Stanford Cars [28], and other datasets of different image sizes. The main contributions of this work are summarized as follows:

- We conduct a layer-wise analysis of CNN's response to input image scale variations. Our investigation reveals that the lower layers of neural networks are highly sensitive to scale changes. This inspires CNN models employing distinct lower layers to extract features for different input scales.
- Based on this finding, we propose Multi-scale Unified Network to enhance the adaptability of CNNs under varying input scales. It comprises multi-scale subnetworks, a unified network, and scale-invariant constraint. Our method can be readily applied to different CNN architectures.
- Our method demonstrates improved performance and computational efficiency in extensive experiments, including multi-scale testing on ImageNet and transfer learning on other datasets of different image sizes, thus enhancing the practicality of CNN models in real-world applications.

The remainder of this paper is organized as follows. Section II provides an overview of the related work; Section III defines the problem; Section IV investigates the layerwise impacts of CNN models on multi-scale input; Section V describes the proposed MSUN in detail. Section VI presents our experimental results, and Section VII offers concluding remarks.

II. RELATED WORK

A. Layerwise analysis of CNNs

CNNs have achieved remarkable results in various visual tasks, but understanding and interpreting CNN models still

present some challenges. To address this, researchers have conducted in-depth, layer-by-layer analyses of CNNs, attempting to understand the behavior of these networks by decoupling the features of different layers. Among these studies, a basic consensus is that the shallow layers of deep learning models capture low-level features such as edges and textures, while the deeper layers capture complex, high-level semantic information [5], [21], [31], [61]. This principle is consistent across a variety of neural networks, including CNNs [6], [40], [48], [70], recurrent neural networks (RNNs) [11], [12], [52], and transformers [17], [45], [57].

Some investigations into the transferability of features across CNN layers revealed interesting results. It was found that initial layers tend to learn more generic features, while the deeper layers become specialized in extracting task-specific characteristics [68]. This concept of hierarchical feature learning has inspired the transfer of features learned by CNNs to disparate tasks [18]. Further, it has been established that a positive correlation exists between the network's depth and its capacity for feature extraction. This underlines the notable proficiency of deeper CNNs in learning intricate representations [53].

In addition to the fundamental functionality of CNNs, many methods have been proposed to visualize and understand their internal dynamics. For example, the deconvolutional method [71] was used to scrutinize the different layers of a CNN. The Deep Inside Convolutional Networks (DICN) [49] offered an in-depth view of CNNs' intermediate activations. The introduction of Network Dissection [3] allowed for quantitative interpretation of individual CNN units, revealing the upper layers' ability to represent object components or even entire objects. Furthermore, guided backpropagation [51] was employed to highlight class-discriminative regions in CNNs, illuminating the distinct roles of different layers.

However, a layer-wise examination of network behavior under scale variation is unexplored, despite its practical importance for addressing the challenges of varying input scales in CNNs. In this work, we use the Centered Kernel Alignment (CKA) to quantitatively analyze different layers under scale changes. Our experiment reveals that in many representative CNN models, the lower layer features exhibit a more pronounced impact from scale changes, thus leading to degraded network performance under scale variations. This insight inspires our method of training different lower layers of the network for multi-scale input.

B. Scale-invariant Feature Extraction

Scale-invariant feature extraction aims to extract features consistent across variable image scales, enhancing the model's robustness to changes in image scale. This concept has been integral to traditional features since the early research, methods such as Scale-Invariant Feature Transform (SIFT) [36] and Speeded Up Robust Features (SURF) [4]. SIFT achieves scale invariance by processing the image in a scale space generated through Gaussian blurring and downsampling of the original image. During this process, SIFT identifies extrema points in the scale space, which serve as keypoints. SURF utilizes

the Hessian matrix for keypoint detection and employs the integral image to compute the Hessian matrix at different scales, significantly improving computational efficiency. As a result, both SIFT and SURF are capable of locating these keypoints regardless of image scale.

After that, Affine-Scale Invariant Feature Transform (ASIFT) extends the scale invariance of SIFT by introducing affine invariance [39]. Maximally Stable Extremal Regions (MSER) provides scale invariance through region-based feature representation [38]. Local Binary Descriptors (LDB) and Binary Robust Invariant Scalable Keypoints (BRISK) employ binary descriptors to improve speed and robustness [32], [67]. These works continuously improve and explore scale invariance in feature extraction, enhancing matching performance and computational efficiency.

Traditional methods have inspired deep learning models to incorporate scale invariance in their design. For instance, Scale-invariant CNN (SiCNN) [65] encodes scale information into the architecture through shared convolutional kernels across scales. The Inception module [53], which uses parallel convolutional layers of varying kernel sizes to capture different scale features, has been adopted widely in popular architectures like GoogLeNet [53] and InceptionV3 [54]. ZoomNet [62] adopts multi-scale feature fusion for learning across scales. The Pyramid Scene Parsing Network (PSPNet) [72] employs pyramid pooling to capture global context information at various scales. Feature Pyramid Networks (FPN) [34] construct a top-down architecture with lateral connections to blend high-level semantic information with low-level spatial information, forming a multi-scale feature pyramid. Atrous convolutions [8], by adjusting the dilation rate, control the effective field of view, capturing context information at varying scales without parameter increase. This technique has seen successful application in the DeepLab architectures [8], [9].

The above models reveal two shortcomings, however. **Firstly**, their performance tends to significantly decrease when the scale of the input images changes. They are not aimed to extract unified features robust to input scale variation, but to provide multi-hierarchy features for handling different scales of objects. This is different from the scale invariance we originally hoped to achieve. **Secondly**, different layers of neural networks have unique functions and characteristics, and these should be considered cooperatively with scale invariance constraints. Our experiments show that the lower layers of the network are more sensitive to scale changes, and they should be prioritized when satisfying scale invariance.

C. Multi-Scale Adaptive CNNs

Supporting multi-resolution input in neural networks has been an issue of active research, as it offers potential improvements in computational efficiency and robustness for neural networks. A direct idea is to train neural networks using images of different resolutions (still resized to fixed-size input, however). which is called multi-scale data augmentations or multi-scale training. This method encourages models to learn features across scales, establishing a widely adopted paradigm [35], [35], [44], [44]. However, training on mixed-scale images

can be detrimental to the performance on standard resolutions. Another method is to learn how to resize images [55]. It can notably improve model performance at a specific resolution by replacing the conventional bilinear interpolation with a learned, CNN-based resizer integrated into the training process. Despite this, the trained resizer model can only adjust images to a certain resolution, exhibiting limited adaptability across different scales.

Some methods aim to balance between computational efficiency and accuracy by altering image resolution and network structure, such as Resolution Adaptive Networks (RANet) [60], Multi-Scale Dense Networks (MSDNet) [23], and Dynamic Resolution Networks (DRNet) [7], adapt the model's architecture and resolution dynamically based on whether the input image is easy or difficult to infer. Among them, RANet downsamples easy-to-judge samples and uses a smaller network for inference, thereby improving its efficiency. DRNet uses a Resolution Predictor to predict the image resolution to be downscaled based on difficulty. MSDNet optimizes computational efficiency on simpler images by downsampling them and predicting based on the output of the network's mid-layers, rather than using the entire network. These methods improve the computation efficiency by adaptively downsampling easy images, but do not consider the scale invariance of input images which are originally multi-scaled or multi-resolution.

In this work, we propose a simple but effective method that can be applied to existing CNNs without complicated modifications. Distinct from previous methods, it considers inherent scale invariance of multi-scale input images in the design of network architecture and training algorithm. The proposed MSUN achieves remarkable improvements in computational efficiency and overall performance in experiments on multiple datasets of different image sizes.

III. PRELIMINARIES

In real-world applications, images input to deep learning models often have variable scales. This necessitates that models maintain robust performance across diverse input scales without retraining. Conventional methods re-size all input images into the same size for convenient processing by neural networks. This may deteriorate the performance on images of variable scales, however.

To assess the model performance across different scales of input, let's consider a standard classification task involving a training dataset D_{train} and a testing dataset D_{test} . In the multi-scale setup, we resize D into a collection of testing sets with varying scale: D_0, D_1, \dots, D_N , corresponding to input sizes R_0, R_1, \dots, R_N . The model is then evaluated on these testing sets to gauge its performance under each size, instead of just evaluating it at the image size consistent with the training set.

We consider two settings for multi-scale experiments:

- **Multi-scale testing:** In this case, the categories C of D_{train} and D_{test} remain the same. Compared to the standard classification task, the model's performance is evaluated on a broader image size range of D_{test} , in different input sizes R_0, R_1, \dots, R_N .

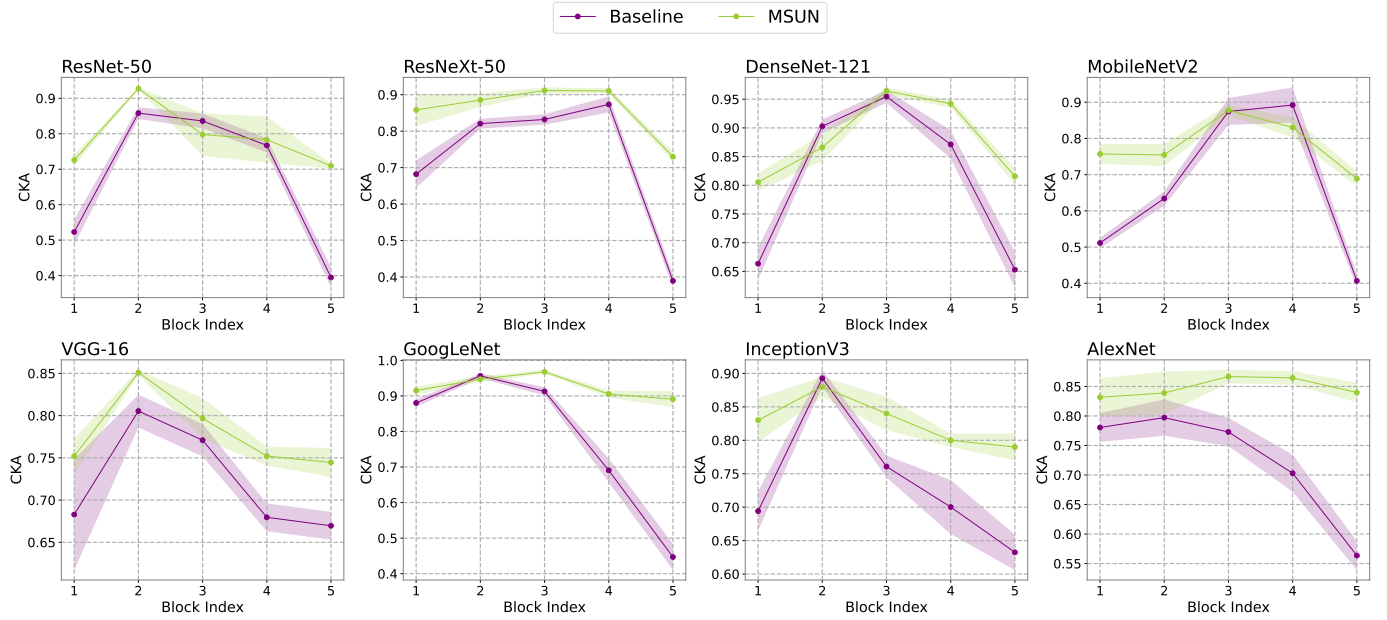


Fig. 2. The layer-wise feature similarity between 32×32 and 224×224 inputs, showing that the lower layers in these CNN models are considerably more sensitive to scale changes. Compared to the baseline, our method (MSUN) maintains a higher CKA between inputs of different input scales, obtaining more robust representations across scale variations.

- **Multi-scale transfer learning:** For a model trained on D_{train} , D_{test} possesses different categories and distributions from D_{train} . This evaluates the transferability of the trained model on datasets of different sizes.

We represent the model with two parts for analysis: a feature extractor \mathcal{F} and a classifier g . The feature extractor, parameterized by θ , encodes the input into a representation as $z = \mathcal{F}(x; \theta)$. In multi-scale testing, the trained \mathcal{F} and g are directly used for evaluation. In multi-scale transfer learning, we train the feature extractor and classifier on the transfer dataset via fine-tuning. For linear evaluation, only g is trained while \mathcal{F} is kept fixed.

IV. LAYER-WISE INVESTIGATION OF CNNs UNDER MULTI-SCALE INPUT

A. Performance Collapse of Scale Variations

Current CNNs maintain uniform image size within a batch during training to take advantage of parallel processing efficiencies. However, in the real world, images present a wide range of sizes, and when a well-trained network is deployed, it is expected to grapple with inputs of varying scales.

Intuitively, there are two strategies for tackling this: apply the CNN directly to the original image size (this needs resizing the training images to match the size of test images), or resize the original image to match the model's input size of training data before inference. We conduct experiments on a range of commonly-used networks, including ResNet [22], ResNeXt [64], DenseNet [24], MobileNetV2 [46], VGGNet [50], GoogLeNet [53], InceptionV3 [54], and AlexNet [30]. To simulate and assess how these models perform when handling varying scale images in real world, the ImageNet test set is resized to different image size, like 32×32 , 128×128 and 224×224 . The results of these two strategies shown in Table I highlight two key findings:

TABLE I

PERFORMANCE EVALUATION OF CNNs ON DIFFERENT INPUT SIZES OF IMAGE NET DATASET. AN ASTERISK (*) SIGNIFIES INFERENCE ON THE ORIGINAL IMAGE SIZE (BY RESIZING TRAINING IMAGES TO THE TEST IMAGE SIZE), WHEREAS NON-ASTERISK COLUMNS INDICATE THAT THE IMAGES ARE RESIZED TO 224×224 . SOME RESULTS ARE MISSING FOR INCEPTION-V3 AND ALEXNET, WHICH DO NOT WORK ON THESE REDUCED IMAGE SIZES.

Models	Input size				
	32x32*	32x32	128x128*	128x128	224x224
ResNet50	4.48	19.64	64.68	68.84	75.18
ResNext50	3.64	25.35	67.63	72.92	77.61
DenseNet121	3.63	21.07	63.61	69.26	74.51
VGG16	3.85	14.35	64.22	67.31	74.32
MobileNet-v2	1.63	16.16	58.70	65.23	71.97
GoogleNet	1.62	15.47	54.91	64.52	69.77
Inception-v3	-	21.41	-	64.88	69.52
AlexNet	-	13.46	37.83	50.53	56.55

First, models inputting images of lower image size result in notable performance drop. This issue exists even in GoogLeNet and InceptionV3, which aim for scale invariance. Lower image size leads to low performance because the image loses many object details in low resolution.

Second, compared to inference at the original image size, resizing images to match the training set image size boosts performance, improving accuracy by 3.09%-12.70% and 10.50%-21.71%. However, this increases the computational overhead of the model.

As shown in Table I, when the input size is reduced from 224×224 to 128×128 , the model performance drops by 4.64%-7.01%, when the input size is further reduced to 32×32 , the models' suffer from performance drop as large as 43.09%-59.97%.

B. Centered Kernel Alignment

To analyze the effects of different layers on model performance changing input scale, we introduce the Centered Kernel Alignment (CKA) metric [15], [27], a widely used method to compare the learned representations across different layers of neural networks. CKA computes the similarity between two sets of features by comparing their centered Gram matrices, which are the inner products of the feature vectors after centering.

Consider two sets of feature representations, $X \in \mathbb{R}^{n \times d_x}$ and $Y \in \mathbb{R}^{n \times d_y}$, where n is the number of samples and d_x and d_y signify the dimensionalities of the features. The first step in the CKA metric computation is to center these feature representations by subtracting their means:

$$\begin{aligned}\tilde{X} &= X - \frac{1}{n}X\mathbf{1}_{n \times n}, \\ \tilde{Y} &= Y - \frac{1}{n}Y\mathbf{1}_{n \times n},\end{aligned}$$

where $\mathbf{1}_{n \times n}$ is an $n \times n$ matrix with all elements equal to $\frac{1}{n}$. The centered Gram matrices, K_X and K_Y , are then calculated as the inner products of the centered feature representations:

$$\begin{aligned}K_X &= \tilde{X}\tilde{X}^T, \\ K_Y &= \tilde{Y}\tilde{Y}^T.\end{aligned}$$

Finally, The CKA metric is computed as the normalized Frobenius inner product of the centered Gram matrices:

$$\text{CKA}(X, Y) = \frac{\langle K_X, K_Y \rangle_F}{|K_X|_F |K_Y|_F}, \quad (1)$$

where $\langle \cdot, \cdot \rangle_F$ denotes the Frobenius inner product, and $|\cdot|_F$ denotes the Frobenius norm.

The value of CKA ranges from 0 to 1, with 0 indicating no similarity between the feature representations and 1 indicating identical feature representations.

C. Understanding the Impact of Scale Variations

To understand the performance associated degradation with scale variations, we initiate a layer-wise inspection using CKA. In particular, we evaluate a convolutional network F divided into five intermediate layers or blocks, denoted as F_1, F_2, F_3, F_4 , and F_5 . We record the outputs, $F_i(x)$, of these intermediate layers and compare the similarity of these outputs under small (32×32) and large (224×224) scale inputs, denoted by X_{32} and X_{224} respectively, using the following equation:

$$\text{CKA}(F_i(X_{32}), F_i(X_{224})) \quad \text{for } i = 1, 2, \dots, 5. \quad (2)$$

The CKA curve offers a quantitative indication of feature variations within the network. Intuitively, a robust model should maintain a high feature similarity under diverse scale inputs. As shown in Figure 2, the curve of a better model should be closer to 1, especially in the final layer. We observe the following phenomena of these CNN models:

- The features of the final layer, which are directly associated with classification performance, show remarkable shifts when dealing with scale variations. This denotes

a lack of robustness in these models, leading to the performance corruption shown in Table I.

- Across these models, it is commonly observed that ***the lower layers are more heavily impacted by scale variations compared to other intermediate layers***. The lower layer features affect the final layer features through forward propagation, thus leading to degradation of final performance

This trend is also in line with previous analyses on CNNs [5], [21], [31]. They suggest that lower layers extract local features such as edges and textures, whereas deeper layers capture more global, semantic features. When the input scale changes, the local details of the image are modified, but the global semantics should stay consistent across scales. Therefore, performance corruption can be attributed to lower layers' sensitivity to scale changes. This motivates our work to handle scale variation in model design.

Our method employs different subnetworks to handle inputs of different scales. It poses consistency in the lower layer features across scales, to enhance the CKA similarity of both lower and final layers is achieved. As illustrated in Figure 2, This denotes an overall improvement in robustness to multi-scale inputs. A detailed description of our method will be provided in Section V.

V. METHOD: MULTI-SCALE UNIFIED NETWORK

A. Overview of the Method

The proposed Multi-scale Unified Network (MSUN) consists of multi-scale subnetworks, scale-invariant constraints, and a unified network. MSUN is compatible with most widely used CNN architectures, including ResNet, DenseNet, ResNext, VGGNet, MobileNetV2, etc. It is designed to provide a more flexible and robust way of handling varying input scales.

The shallow layers of MSUN are partitioned into multi-scale subnetworks designed to handle different input scales divided into rough categories such as large, medium, and small. The subnetworks independently extract low-level features, to overcome the sensitivity to scale variations. To extract robust high-level features, we enforce scale-invariant constraints to ensure consistency in the features extracted across different input scales, which is crucial in enhancing the network's resilience to changes in scale. The extracted low-level features are then processed through a common deep network to extract high-level semantic features. In the inference phase, the subnetwork aligning with the input image's scale is selected, avoiding the computational costs of rescaling input image, especially into a larger size.

Our method is illustrated in Figure 3. It differs from the Vanilla model (which has fixed input size) and multi-scale training method (which transforms multi-scale images into the same size in training and inference) in that it has multiple lower-layer subnetworks and a unified high-level network for enhancing scale invariance and avoiding rescaling input images to a fixed size.

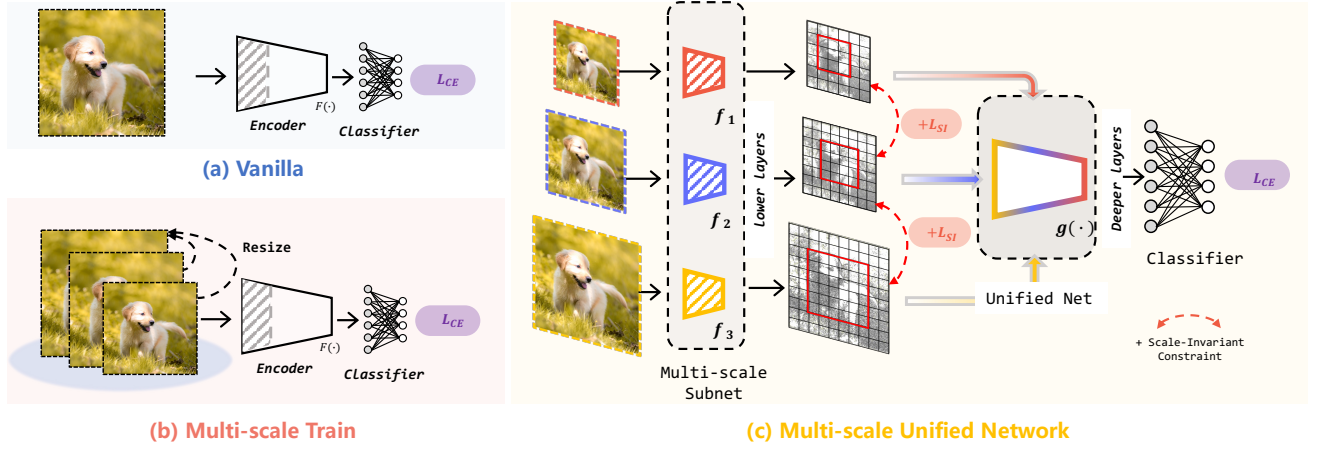


Fig. 3. Illustration of the Vanilla model [22], [24], [46], [50], multi-scale training, and our method. MSUN has the lower layers divided into multi-scale subnets, which are unified in upper layers incorporating a scale-invariance constraint.

B. Multi-scale Subnet and Unified Net

To apply MSUN on a standard CNN model F , which consists of lower layers f and deeper layers g , expressed as $\mathcal{F}(x) = g(f(x))$, parallel subnetworks are used to replace the lower layers f , aiming to extract features at varying scales. In this paper, we utilize three quantized scales (large, medium, and small) which turn out to perform sufficiently well. The large-scale subnetwork aligns with the shallow network f in the original model. For the other two scales, we substitute the large convolutions with smaller ones and discard some max-pooling layers, intending to make it adapt to smaller input sizes. Subsequently, the unified network g extracts high-level semantic features from each scale subnetwork's output. The overall feature extraction process of the ordinary CNN model \mathcal{F} and the MSUN $\hat{\mathcal{F}}$ are formulated as:

$$\mathcal{F}(x) = g(f_N(x_N)), \quad (3)$$

$$\hat{\mathcal{F}}(x) = [g(f_1(x_1)), g(f_2(x_2)), \dots, g(f_N(x_N))], \quad (4)$$

where x_i represents the i -th quantized scale of input image and f_i denotes the subnetwork corresponding to the i -th scale. MSUN assumes N scales ($N = 3$ in our paper), while the ordinary CNN directly takes the largest scale x_N for high performance.

Given an input x with a certain size $R(x)$ in the inference stage, the model resizes the image to the quantized scale $R(x_i)$ that closely matches a subnetwork. The model only needs to calculate the low-level features at this scale, which aligns with the computation process of the original CNN model:

$$\hat{\mathcal{F}}_{\text{test}}(x) = g(f_i(x_i)) \quad (5)$$

$$i = \arg \min_{i=1}^N (|R(x) - R(x_i)|). \quad (6)$$

The architecture of multi-scale subnetworks and a unified net provides a more flexible approach for handling varying input scales. This approach enables calculations to be performed at a size much closer to that of the original image, significantly improving computational efficiency when dealing with multi-scale inputs. Consequently, this flexibility also improves model

Algorithm 1 Multi-Scale Unified Network Training

- 1: **Input:** CNN model \mathcal{F} , training images x , labels y
- 2: Transform F to subnetworks f_1, f_2, \dots, f_n and unified network g
- 3: **for** each epoch **do**
- 4: **for** each mini-batch **do**
- 5: Calculate L_{CE} for each scale x_i by forward-passing the input through f_i and g
- 6: Calculate L_{SI} by computing $D(f_i(x), f_j(x_s))$ for all pairs of scales
- 7: Calculate overall loss $L = L_{CE} + \max(\lambda, L_{SI})$
- 8: Backpropagate the gradients and update the parameters of f_i and g
- 9: **end for**
- 10: **end for**

performance due to the better adaptability to input scale variation.

C. Scale-Invariant Constraint

To make features extracted by the multi-scale subnetworks consistent across scale space, we introduce a scale-invariant constraint inspired by traditional features extensively used in the past, such as SIFT [36] and SURF [4], through the creation of a scale space and assuming invariance across difference scales.

For achieving scale invariance in the unified high-level layers of MSUN, we introduce the scale-invariant constraint (SI) as a regularization term, $L_{SI}(f_1, f_2, \dots, f_n)$, in the loss function. In this context, x_i represents an image x resized to the i -th quantized scale, while f_i denotes the shallow subnetwork corresponding to the i -th scale. The SI is calculated as:

$$L_{SI}(f_1, f_2, \dots, f_n) = \sum_{i=1}^{n-1} \sum_{j=i+1}^n D(f_i(x), f_j(x_s)), \quad (7)$$

where $D(\cdot, \cdot)$ represents a distance metric (e.g., Euclidean distance) that measures the discrepancy between the features extracted by different subnetworks.

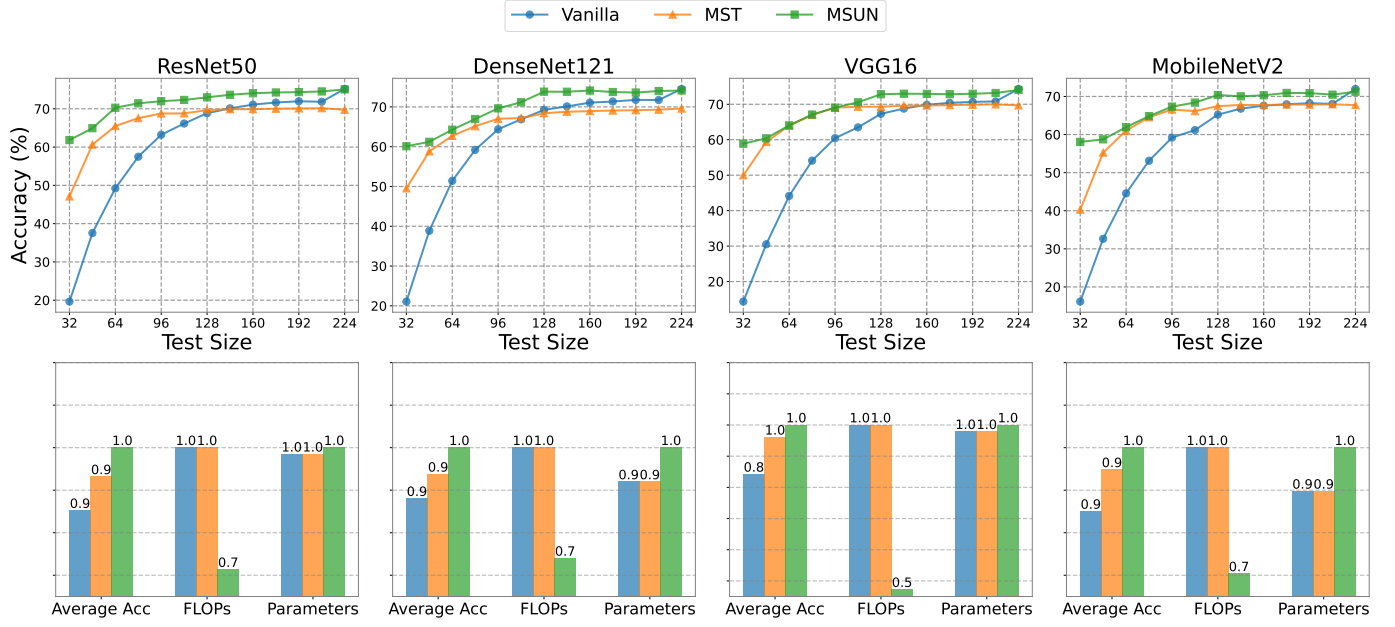


Fig. 4. Multi-scale testing on ImageNet spanning from 32×32 to 224×224 image size with a stride of 16. (a) The model’s accuracy curves at each input size. (b) The model’s average accuracy, average FLOPs, and total model parameters across these sizes. Our method demonstrates significant accuracy improvements and reduced FLOPs, mitigating the model’s performance breakdown at lower image scales.

The overall loss function for training MSUN models is:

$$L = \max(L_{SI}(f_1, f_2, \dots, f_n), \lambda) + \sum_{i=1}^N L_{CE}(g(f_i(x)), y), \quad (8)$$

where L_{CE} denotes the cross-entropy loss function for classification, y represents the ground truth labels of x , and λ is a hyperparameter for balancing task-specific loss and the scale-invariant constraint.

Algorithm V-B provides the pseudo-code for our method. By incorporating the SI constraint into the loss function, the CNN model is encouraged to learn features robust to scale variation, leading to improved performance when dealing with images of varying scales during inference.

VI. EXPERIMENTS

A. Evaluation Metrics

The performance metrics for evaluating models under multi-scale inputs are based on the Learning to Resize method [55] and other related works [1], [56]. We use three main metrics to assess our method:

Average Accuracy: This metric calculates the mean of accuracies achieved across all test input sizes: $\bar{A} = \frac{1}{T} \sum_{t=1}^T A_t$, where A_t is the classification accuracy evaluated on the current test set at the t -th scale.

Parameters: The model complexity is measured by the number of trainable parameters in the model.

FLOPs: The metric Floating Point Operations Per Second (FLOPs) is used to evaluate the computational cost of the model. FLOPs of each layer is defined as $FLOPs = 2 \times n \times m \times k^2$, where n denotes the number of input feature maps, m denotes the number of output feature maps, and k represents the size of the convolutional kernel.

B. Setup

Datasets: Our experiments used diverse datasets, with ImageNet [16] for primary training. Validation images were resized to 32×32 to 224×224 (step 16) pixels in multi-scale testing. The model trained on ImageNet was transferred to datasets CIFAR-10 [29], CIFAR-100 [29], STL-10 [14], Caltech-101 [20], Fashion-MNIST [63], Oxford 102 Flowers [41], Oxford-IIIT Pets [43], Stanford Cars [28], FGVC Aircraft [37], Describable Textures Dataset (DTD) [13], and RAF-DB [33], spanning image sizes of 28×28 to 224×224 pixels. We used the first train/test split for DTD, and random 30 images per class for Caltech-101 testing.

Backbone Networks: Our method is validated on popular CNN architectures including ResNet-50 [22], DenseNet-121 [24], VGG-16 [50], and MobileNet-v2 [46]. We compare MSUN with the original models (Vanilla), and models with multi-scale training (MST). These CNNs are utilized in multi-scale testing and transfer learning. Ablation studies are conducted using ResNet-50.

Implementation Details: Networks are trained using the Stochastic Gradient Descent (SGD) optimizer [30] with an initial learning rate of 0.1, momentum of 0.9, weight decay of $2e-5$, and a batch size of 128 per GPU. The learning rate scheduler employed is LinearWarmupCosineAnnealingLR with a 5-epoch warm-up and start/minimum learning rates at 0.01 of the initial rate. In our network architecture, we employ three quantized scales: large (224×224), medium (128×128), and small (32×32). Networks are trained for 90 epochs, with MobileNetV2 extended to 300 epochs. Linear-probe and fine-tuning run for 30 epochs. Other settings like data transformation follow PyTorch’s official implementation. *Our code will be made public once this paper is accepted, and more implementation details can be found in the code.*

TABLE II

MULTI-SCALE TESTING ON IMAGENET ACROSS INPUT SIZES FROM 32×32 TO 224×224 WITH A STRIDE OF 16. THE MEASURES ASSESSED INCLUDE THE ACCURACY AT EACH SIZE, AVERAGE FLOPS, AND THE NUMBER OF MODEL PARAMETERS.

Methods		Params (↓)	FLOPs (↓)	Input size												
				32	48	64	80	96	112	128	144	160	176	192	208	224
ResNet50	Vanilla	25.6M	3.28×10^{10}	19.64	37.55	49.22	57.48	63.22	66.15	68.84	70.11	71.09	71.64	71.96	71.84	75.18
	MST	25.6M	3.28×10^{10}	47.11	60.65	65.49	67.56	68.77	68.80	69.67	69.89	69.90	70.02	70.10	70.15	69.76
	MSUN	26.0M	3.05×10^{10}	61.83	64.92	70.28	71.43	71.98	72.31	72.99	73.66	74.07	74.26	74.35	74.53	75.06
DenseNet 121	Vanilla	8.0M	2.28×10^{10}	21.07	38.86	51.42	59.20	64.38	66.87	69.26	70.12	71.07	71.36	71.76	71.73	74.51
	MST	8.0M	2.28×10^{10}	49.53	58.83	62.73	65.15	67.03	67.18	68.40	68.78	68.94	69.09	69.16	69.31	69.59
	MSUN	8.7M	1.99×10^{10}	60.11	61.23	64.27	66.95	69.63	71.17	73.83	73.81	74.11	73.74	73.61	73.99	74.12
VGG16	Vanilla	138.0M	1.24×10^{11}	14.35	30.51	44.15	54.11	60.45	63.48	67.31	68.78	69.87	70.40	70.67	70.80	74.32
	MST	138.0M	1.24×10^{11}	49.96	59.41	63.96	66.97	69.07	69.31	69.30	69.60	69.64	69.75	69.88	69.97	69.68
	MSUN	141.0M	1.04×10^{11}	58.88	60.40	64.05	67.10	69.04	70.55	72.83	72.98	72.94	72.83	72.96	73.19	74.03
MobileNet V2	Vanilla	3.5M	2.46×10^9	16.16	32.65	44.57	53.14	59.20	61.17	65.23	66.80	67.58	67.95	68.24	68.05	71.97
	MST	3.5M	2.46×10^9	40.29	55.27	61.04	64.53	66.57	66.15	67.47	67.76	67.75	67.88	67.86	67.94	67.75
	MSUN	3.9M	2.28×10^9	58.07	58.74	61.93	64.85	67.33	68.40	70.37	70.04	70.31	70.93	70.88	70.48	71.24

C. Comparative results

This section discusses the results of experiments on multi-scale testing, linear-probe transfer, and fine-tuning transfer settings.

Multi-scale Testing: In multi-scale testing (MST), the images in the dataset are rescaled into different sizes. All the rescaled images in training set are upsampled to the original size and used to train the model with fixed input size. When an image of smaller size is tested, it is upsampled to the standard input size of the model. Figure 4 and Table II show the test accuracies on ImageNet dataset with different input sizes. As results, MST surpasses Vanilla models at smaller input sizes, but sacrifices 4.03-5.20% accuracy on larger sizes like 224×224 . This is because the Vanilla model is trained with images of one size only, while in MST, the model is trained using images of multiple sizes. Our method MSUN outperforms both Vanilla and MST across most input sizes, especially small sizes. For instance, in the case of ResNet-50, when employing MSUN, achieves an accuracy 61.83% at the size of 32×32 pixels, which is higher than MST's 47.11% and the Vanilla model's 19.64%. Similarly, DenseNet-121, VGG-16, and MobileNetV2 exhibit an accuracy boost of 8.92 - 17.78% compared to MST, and 39.04 - 44.53% when compared to Vanilla models. At the largest size 224×224 , the MSUN models experience only a slight drop of 0.12-0.73% compared to the Vanilla models. In summary, with a slight parameter increase of 1.56-11.43%, MUSN achieves an 8.39-10.97% rise in average accuracy and a 7.01-16.13% cut in average FLOPs for input sizes ranging from 32×32 to 224×224 .

Linear-Probe Evaluation: During linear evaluation, the feature extractor is fixed after training on ImageNet and linear classifiers are trained on target datasets. As shown in Table III, MST and MSUN exhibit significant improvements across the majority of models and datasets, indicating that enhancing multi-scale adaptability considerably boosts the transferability of models. Specifically, on lower image size datasets like CIFAR-10, CIFAR-100, Fashion-MNIST, and RAF-DB, MST and MSUN achieve 1.46-17.42% and 0.71-16.48% accuracy

improvement respectively. For other datasets, MST boosts performance by 0.10-6.44% in part of datasets and models but counters a 0.03-4.03% drop in others. MSUN exhibits robust performance, achieving 0.18-6.96% improvements and declining 2.71% only when using MobileNetV2 on the DTD dataset. Moreover, it reduces average FLOPs by 3.55-8.45% across these datasets.

Fine-Tuning Transfer: In this scenario, both the encoder and classifier of the model pre-trained on ImageNet are retrained together on the target dataset. As shown in Table III, the disparity in accuracy between MST, MSUN, and standard models diminishes. Vanilla models exhibit a marginal advantage of 0.35-5.46% on datasets such as DTD, RAF-DB, and Cars. MST improves accuracy by 0.10-7.69% on the first six datasets, but reduces by 0.42-5.46% on the remains. MSUN exhibits a 0.22-8.40% improvement across all datasets, except for a minor 0.20-0.36% drop on some models in the Cars and DTD dataset, demonstrating superior transferability. Additionally, it flexibly accommodates multi-scale inputs and reduces computational costs during retraining on the transfer datasets.

D. Ablation study

We analyze ablation studies utilizing the ImageNet dataset with ResNet-50 as the backbone model. The architecture of MSUN can be represented as B -blocks- S -subnets, where each sub-network is composed of a number of blocks (denoted as B), and the total number of sub-networks is denoted as S . For our implementation, we have employed one block and three sub-networks in our standard model, which is depicted as Res50- $B1$ - $S3$. The ablation study consists of the following parts:

Multi-scale Subnet Assessment: We analyzed subnetworks f_1 , f_2 , and f_3 , specialized for small, medium, and large-scale inputs respectively, to gauge their individual impact on performance. The results of multi-scale tests on ImageNet can be found in Table IV and Figure 5. f_1 achieves 24.1-34.4% better performance for small scales input, such as

TABLE III

COMPARISON OF TRANSFER LEARNING PERFORMANCE USING OUR METHOD, VANILLA BASELINES, AND MULTI-SCALE TRAINING, EVALUATED OVER 11 NATURAL IMAGE DATASETS. THE INPUT SIZE VARIES FROM 28×28 TO 224×224 , DEPLOYING MODELS PRE-TRAINED ON IMAGENET.

Methods	FLOPs (\downarrow)	DataSets											
		CIFAR-100	Pets	CIFAR-10	Cars	STL-10	Fashion	RAF-DB	Aircraft	Caltech	DTD	Flowers	
<i>Linear-Probe:</i>													
ResNet50	Vanilla	3.28×10^{10}	57.55	89.95	77.57	52.85	93.98	87.82	52.12	20.97	83.93	62.61	87.24
	MST	3.28×10^{10}	74.03	86.32	91.30	52.57	92.89	90.05	59.81	28.10	84.42	62.61	86.89
	MSUN	3.12×10^{10}	74.97	90.48	92.40	54.88	94.86	90.18	60.37	31.73	84.52	63.30	88.37
DenseNet 121	Vanilla	2.28×10^{10}	58.99	90.41	79.39	56.24	93.58	89.20	56.10	23.67	84.65	63.62	88.51
	MST	2.28×10^{10}	74.22	90.14	91.67	56.40	94.63	90.67	58.41	32.72	85.58	63.19	88.57
	MSUN	2.02×10^{10}	74.55	90.82	91.88	58.22	94.70	90.76	60.11	33.54	85.42	63.80	89.88
VGG16	Vanilla	1.24×10^{11}	58.50	90.03	80.79	60.07	93.30	91.47	63.66	31.16	81.35	67.32	87.30
	MST	1.24×10^{11}	74.65	89.35	91.85	56.04	95.42	92.82	64.37	34.33	81.39	64.63	84.89
	MSUN	1.13×10^{11}	74.87	90.24	91.90	60.75	95.50	93.33	65.12	34.45	82.31	68.11	88.66
MobileNet V2	Vanilla	2.46×10^9	51.35	88.56	74.99	51.34	86.62	87.54	52.31	23.91	83.86	61.86	87.54
	MST	2.46×10^9	67.49	88.28	87.24	50.88	93.06	89.46	56.81	30.38	82.71	60.16	87.53
	MSUN	2.31×10^9	67.98	89.82	87.75	51.63	93.58	89.72	58.35	31.32	84.00	62.32	89.29
<i>Fine-tuned:</i>													
ResNet50	Vanilla	3.28×10^{10}	80.97	85.04	96.37	88.70	93.30	95.12	82.64	48.44	83.83	60.64	87.22
	MST	3.28×10^{10}	82.63	84.39	96.61	83.77	93.70	95.43	81.23	42.98	88.94	60.68	88.42
	MSUN	3.12×10^{10}	82.83	86.42	96.63	88.39	94.26	95.51	83.12	49.31	90.05	61.29	89.44
DenseNet 121	Vanilla	2.28×10^{10}	81.46	85.61	96.23	89.00	93.07	95.24	80.80	49.94	85.54	60.35	87.37
	MST	2.28×10^{10}	82.03	86.43	96.98	87.35	94.76	95.65	82.53	48.92	89.44	60.00	90.31
	MSUN	2.02×10^{10}	82.75	86.77	96.81	89.36	94.83	95.70	83.04	50.74	89.94	60.15	90.63
VGG16	Vanilla	1.24×10^{11}	77.13	88.04	95.43	88.81	93.85	95.44	83.05	51.95	74.75	63.62	86.51
	MST	1.24×10^{11}	79.84	88.26	96.25	87.16	94.95	95.54	82.63	51.38	82.44	62.55	89.82
	MSUN	1.13×10^{11}	80.97	88.54	96.70	89.21	94.87	95.88	82.69	52.97	83.15	63.84	89.98
MobileNet V2	Vanilla	2.46×10^9	78.25	82.94	94.82	87.94	90.71	94.88	81.58	48.59	81.58	61.06	87.64
	MST	2.46×10^9	80.93	83.95	95.67	86.05	92.90	94.99	81.03	48.23	87.72	61.81	89.14
	MSUN	2.31×10^9	80.49	84.10	95.95	87.98	93.24	94.69	82.10	49.31	88.11	62.66	89.76

TABLE IV

THE ACCURACY AND FLOPs OF EACH SUBNETWORK ACROSS DIFFERENT INPUT SIZES. THE MODEL'S FIRST, SECOND, AND THIRD ROWS CORRESPOND TO f_1 , f_2 , AND f_3 , RESPECTIVELY.

Methods	FLOPs (\downarrow)	Input size						
		32	64	96	128	160	192	224
ResNet50	2.84×10^{10}	61.8	61.7	61.5	60.0	60.5	60.4	60.5
	2.92×10^{10}	37.1	70.3	72.0	73.0	72.8	72.3	73.7
	3.28×10^{10}	34.5	61.8	68.0	70.0	74.1	74.3	75.1
DenseNet 121	1.60×10^{10}	60.1	60.5	60.1	60.2	60.1	60.8	60.5
	1.89×10^{10}	36.0	62.7	67.0	73.8	73.6	73.6	73.8
	2.28×10^{10}	33.2	59.8	65.5	69.9	74.0	74.0	74.1
VGG16	8.68×10^{10}	58.9	58.5	58.9	57.9	58.9	58.1	58.9
	9.83×10^{10}	28.4	59.0	68.0	72.8	72.5	72.4	72.8
	1.24×10^{11}	27.6	53.4	65.0	68.7	72.9	73.0	74.0
MobileNet V2	2.02×10^9	58.1	57.8	58.1	58.1	58.1	58.0	58.1
	2.21×10^9	25.7	59.9	64.3	70.4	70.1	70.1	70.4
	2.46×10^9	23.7	51.9	51.2	53.9	70.7	70.9	71.2

32×32 . Similarly, f_2 performs 1.5-8.5% better in the mid-scale range of 64-128 and f_3 excels by 0.4-2.1% for large scales between 160-224. The model adeptly handles varying

TABLE V

THE ACCURACY OF DIFFERENT TEST SIZES UNDER IMAGENET MULTI-SCALE TESTING AND MODEL PARAMETERS, COMPARING DISTINCT MSUN CONFIGURATIONS.

Methods	Params (\downarrow)	Input size						
		32	64	96	128	160	192	224
Res50-B0-S3	25.6M	48.4	67.3	70.0	71.6	73.1	73.3	73.7
Res50-B2-S3	28.4M	62.5	70.7	72.8	75.3	74.8	75.4	75.6
Res50-B3-S3	42.6M	64.6	71.3	73.1	75.3	74.8	75.8	75.9
Res50-B1-S2	25.8M	36.0	62.7	67.0	73.8	73.6	73.6	73.8
Res50-B1-S4	26.2M	62.2	70.8	72.2	73.4	74.3	74.5	75.2
Res50-B1-S5	26.4M	62.2	70.9	72.5	73.5	74.5	74.6	75.2
Res50-B1-S3	26.0M	61.8	70.3	72.0	73.0	74.1	74.3	75.1

input scales by utilizing multi-scale subnets derived from the network's lower layers. During inference, input is resized to the closest input scale of subnetworks, for extracting low-level features, as demonstrated by the green curve in Figure 5. Additionally, f_1 , f_2 reduces FLOPs by 13.41-31.77% and 10.16-19.18% compared to a standard model (f_3), offering significant computational savings.

Examining MSUN Configurations: When employing our

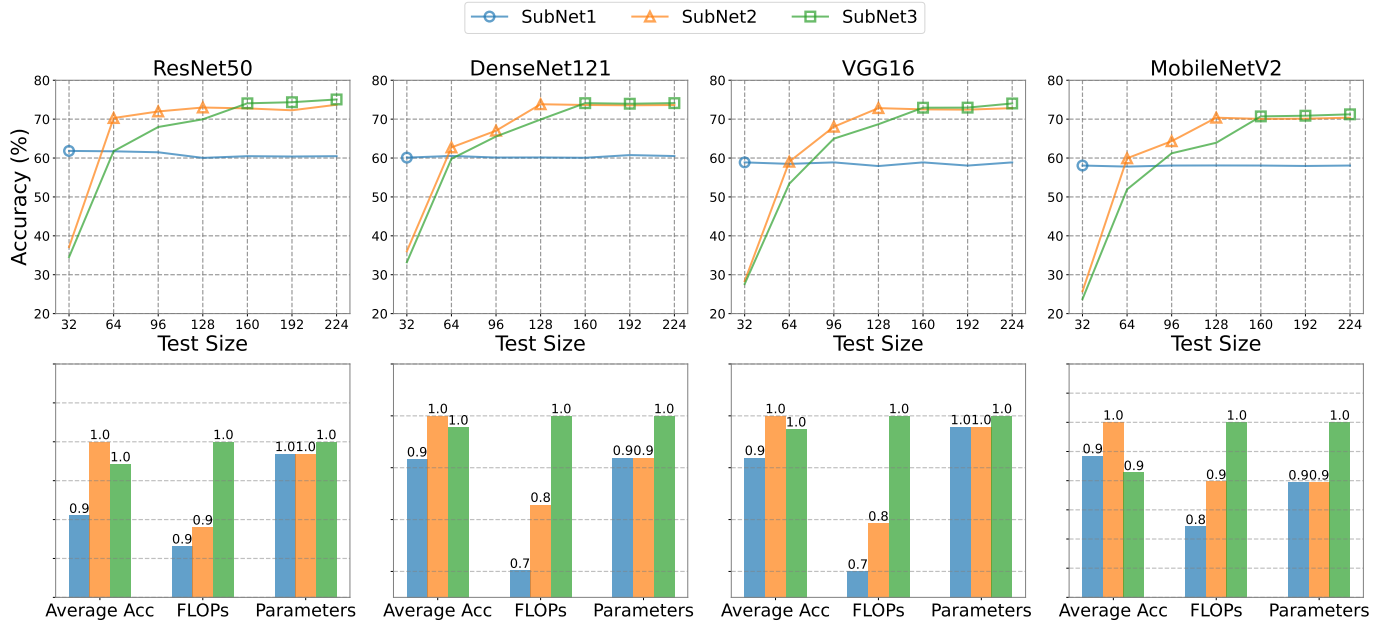


Fig. 5. Comparison of multi-scale subnetworks. Tick marks denote optimal accuracy at each test size. (a) the accuracy curves with different input sizes. (b) Mean accuracy, FLOPs, and total parameters across these inputs.

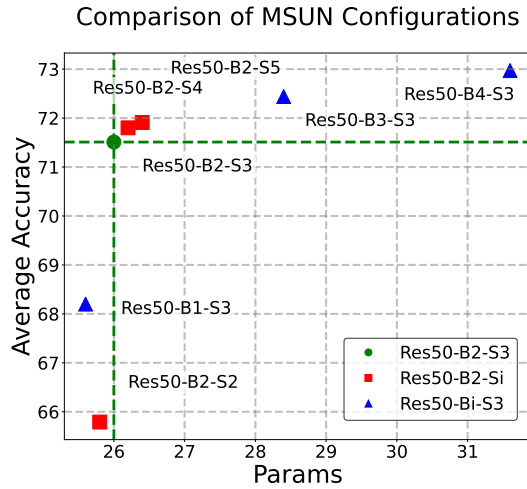


Fig. 6. The average accuracy and model parameters using different MSUN configurations. The red and purple lines indicate the parameters of the original model and the maximum achievable accuracy. Resnet50-B1-S3 maintains a good balance between parameters and accuracy.

method, the CNN is decomposed into multi-scale subnetworks and a unified network. The model's configuration is defined by two primary factors: the number of blocks within each subnetwork and the total number of subnetworks employed. We tested ResNet50 in various settings, between 0 and 3 blocks and 2 to 5 subnetworks. The results of these tests are presented in Table V and Figure 6. It is shown that when increasing the number of blocks within a subnetwork, we observed that the MSUN approaches its upper bound, which is obtained by training an individual model for each image size. However, increasing the number of blocks also leads to a corresponding parameter increase. Notably, with just a single block, the model achieved a performance increase of 19.7% with only a 1.56% increase in parameters. More blocks increase in parameters ranged from 10.94-66.41%, resulting in performance improvements of 20.96-21.84%. Likewise,

TABLE VI
THE AVERAGE ACCURACY ON IMAGENET MULTI-SCALE TESTING AND MODEL PARAMETERS, COMPARING USE VS. NOT USE MULTI-SCALE SUBNET, UNIFIED NET, AND SCALE-INVARIANCE CONSTRAINT.

Methods	SI	SNet	UNet	Params (↓)	Accuracy (↑)
MST	×	×	×	25.6M	66.76
MST+SI	✓	×	×	25.6M	66.95
SNet	×	✓	×	76.7M	73.39
SNet+SI	✓	✓	×	76.7M	72.84
SNet+UNet	×	✓	✓	26.0M	70.31
SNet+UNet+SI	✓	✓	✓	26.0M	71.67

Increasing the number of subnetworks also raises parameters and complexity. With two subnetworks, there is a 0.78% increase in parameters while achieving 11.32-24.31% performance gains on some input scales when compared to Vallina model. However, it results in a performance drop of 2.38% on image size of 224×224 (73.80% versus 75.18%). At block setting B1, increasing subnetworks from S2 to S5 improves the performance by 5.72-6.12% and parameters by 0.77-2.32%, and achieves accuracy comparable to the Vanillina model on 224×224 size.

Impact of Multi-scale Subnet, Unified Net, and SI: We examined MSUN components, including the multi-scale subnetwork (SNet), unified network (UNet), and SI constraint, using the Res50-B1-S3 configuration. The average accuracy from 32×32 to 224×224 and parameter count are shown in Table VI. It is evident that using both Snet and Unet results in slight parameter increase and large performance gain. Excluding Unet prevents sharing of networks across scales, resulting in 73.39% accuracy but with a 199.61% parameter increase. Combining Snet with Unet improves performance by 3.55% with only a 1.56% increase in parameters. Implementing the

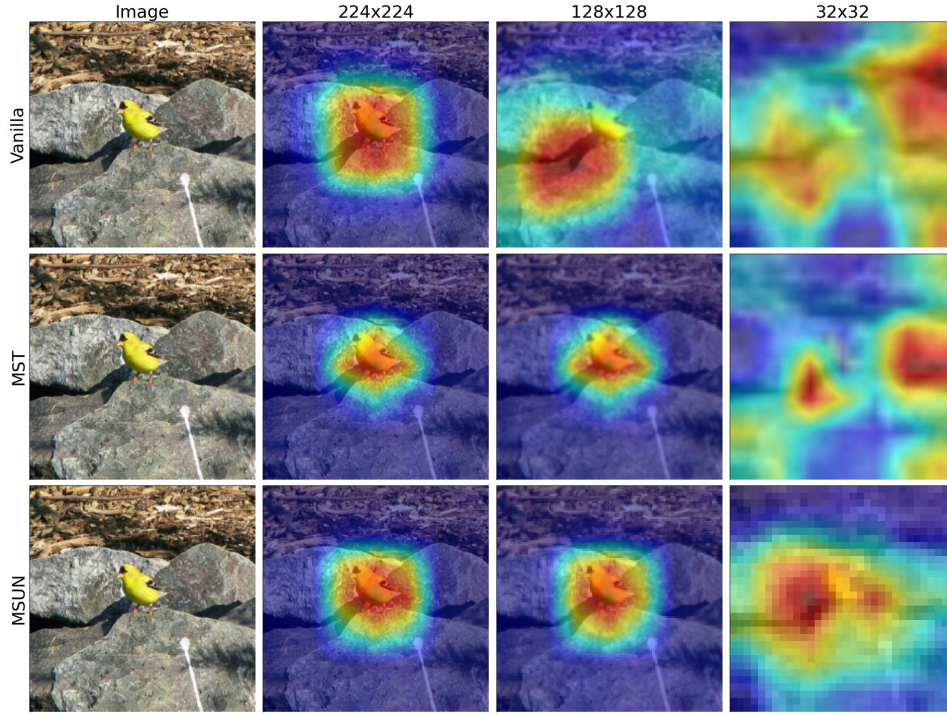


Fig. 7. Grad-CAM visualizations reveal that ResNet50 models pre-trained on ImageNet focus differently depending on input image size. The Vanilla model's attention region becomes inconsistent when the image size changes. MST's focus shifts relative to the Vanilla model, while MSUN retains consistent attention across different input sizes, aligning with the Vanilla model's focus on 224×224 image size.

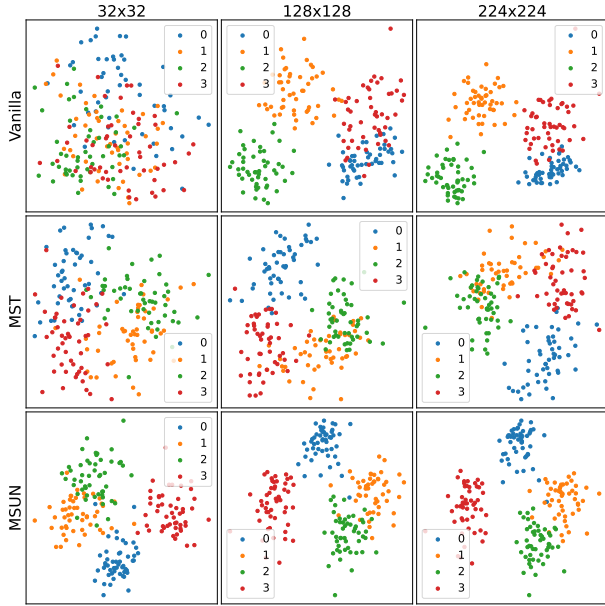


Fig. 8. PCA visualizations with a pre-trained ResNet50 on ImageNet. Vanilla confuses on 32×32 image size, MST alters feature distribution, and MSUN maintains discriminative capabilities across different image size.

SI constraint increases Snet+Unet accuracy from 70.31% to 71.67%. However, using the constraint alone (without SNet and UNet) only yields a marginal improvement of 0.19% (MST versus MST+SI). results indicate that the components SNet, UNet, and SI are crucial for improving the model's performance in multi-scale scenarios. Particularly, the UNet results in reduced parameter complexity while maintaining high performance.

E. Further Analysis and Discussion

Visualization of attention area. Gaining insights into how models allocate attention to distinct areas within images is essential for assessing their robustness across varying image size. To this end, we employ Gradient-weighted Class Activation Mapping (Grad-CAM) as an analytical visualization tool to examine the model's focus on particular regions during decision-making. Grad-CAM is defined as follows:

$$L_{\text{Grad-CAM}}^c = \text{ReLU} \left(\sum_k \alpha_k^c A^k \right), \quad (9)$$

where A^k is the features in the k -th channel of the last layer. α_k^c is how much this feature affects class c . ReLU keeps only positive features. As shown in Figure 7, we use Grad-CAM on MSUN, Vanilla, and MST at 224×224 , 128×128 , and 32×32 image size. The following phenomena are observed:

- MSUN is highly robust to image size changes even on a lower resolution of 32×32 , where the focus areas largely overlap with those on the standard 224×224 size with Vanilla.
- MST demonstrates consistency on 128×128 image size but shows some defocus in the attention area on the smaller 32×32 size. The attention region of the MST model differs largely from that of the Vanilla model.
- The attention focus area of Vanilla model appears highly sensitive to image size changes. While the model performs reliably at the 224×224 standard size, it loses focus consistency at lower size, indicating limited robustness.

In summary, MSUN shows high robustness over various image size, albeit with slight modifications in focus regions relative to the Vanilla model on large input size.

Visualization of feature space. Through PCA visualization, we compared the feature spaces of the models at different input scales in Figure 8. In the feature space of the Vanilla model on 224×224 size, the features of different classes are well separated, but this discriminability degrades notably on 32×32 size. MST mitigates this confusion on 32×32 size, but also distort the feature landscape of the Vanilla model at higher image size, like 224×224 and 128×128 , resulting in lower discrimination. Section 6.1’s experimental results show that this alteration impairs accuracy at elevated image size. In contrast, the MSUN model retains feature separation comparable to the Vanilla model at the 224×224 image size and remains robust across multiple input scales.

VII. CONCLUSION

To improve the robustness of features across variable input image scales, we propose Multi-Scale Unified Network (MSUN) —a restructuring of CNNs into multi-scale subnetworks within a unified network, guided by a scale-invariant constraint. MSUN ensures feature consistency, maintains high performance across different image scales, and significantly reduces computational overhead compared to multi-scale testing and training-test with a fixed large image size. The framework is readily applicable to various CNN architectures. We validated the effectiveness and superiority of the proposed method with a range of common CNN architectures on a number of datasets of various image sizes. Besides image classification evaluated in this paper, we expect that the proposed network can also apply to other computer vision tasks such as object detection, which deals with object regions of highly variable scales. In the future, we will also consider the multi-scale robustness design of other neural network architectures such as the transformer.

REFERENCES

- [1] Bilal Alsallakh, David Yan, Narine Kokhlikyan, Vivek Miglani, Orion Reblitz-Richardson, and Pamela Bhattacharya. Mind the pool: Convolutional neural networks can overfit input size. In *The Eleventh International Conference on Learning Representations*, 2023.
- [2] Junjie Bai, Biao Gong, Yining Zhao, Fuqiang Lei, Chenggang Yan, and Yue Gao. Multi-scale representation learning on hypergraph for 3d shape retrieval and recognition. *IEEE Transactions on Image Processing*, 30:5327–5338, 2021.
- [3] David Bau, Bolei Zhou, Aditya Khosla, Aude Oliva, and Antonio Torralba. Network dissection: Quantifying interpretability of deep visual representations. *Proceedings of the IEEE Conference on Computer Vision and Pattern Recognition*, pages 6541–6549, 2017.
- [4] Herbert Bay, Tinne Tuytelaars, and Luc Van Gool. Surf: Speeded up robust features. In *Computer Vision—ECCV 2006: 9th European Conference on Computer Vision, Graz, Austria, May 7–13, 2006. Proceedings, Part I 9*, pages 404–417. Springer, 2006.
- [5] Yoshua Bengio, Aaron Courville, and Pascal Vincent. Representation learning: A review and new perspectives. *IEEE Transactions on Pattern Analysis and Machine Intelligence*, 35(8):1798–1828, 2013.
- [6] Joan Bruna and Stéphane Mallat. Invariant scattering convolution networks. *IEEE Transactions on Pattern Analysis and Machine Intelligence*, 35(8):1872–1886, 2013.
- [7] Jinjin Chen, Xifeng Pan, Yu-Kun Lai, and Chao Tang. Dynamic relu. In *Proceedings of the IEEE/CVF Conference on Computer Vision and Pattern Recognition*, pages 11–20, 2020.
- [8] Liang-Chieh Chen, George Papandreou, Iasonas Kokkinos, Kevin Murphy, and Alan L. Yuille. Deeplab: Semantic image segmentation with deep convolutional nets, atrous convolution, and fully connected crfs. *IEEE Transactions on Pattern Analysis and Machine Intelligence*, 40(4):834–848, 2018.
- [9] Liang-Chieh Chen, Yukun Zhu, George Papandreou, Florian Schroff, and Hartwig Adam. Encoder-decoder with atrous separable convolution for semantic image segmentation. In *Proceedings of the European Conference on Computer Vision (ECCV)*, pages 801–818, 2018.
- [10] Shaofeng Chen, Yang Cao, Yu Kang, Pengfei Li, and Bingyu Sun. Deep feature representation based imitation learning for autonomous helicopter aerobatics. *IEEE Transactions on Artificial Intelligence*, 2(5):437–446, 2021.
- [11] Kyunghyun Cho, Bart van Merriënboer, Dzmitry Bahdanau, and Yoshua Bengio. Learning phrase representations using rnn encoder–decoder for statistical machine translation. *arXiv preprint arXiv:1406.1078*, 2014.
- [12] Junyoung Chung, Caglar Gulcehre, KyungHyun Cho, and Yoshua Bengio. Empirical evaluation of gated recurrent neural networks on sequence modeling. *arXiv preprint arXiv:1412.3555*, 2014.
- [13] Mircea Cimpoi, Subhransu Maji, Iasonas Kokkinos, Sammy Mohamed, and Andrea Vedaldi. Describing textures in the wild. In *Proceedings of the IEEE Conference on Computer Vision and Pattern Recognition*, pages 3606–3613, 2014.
- [14] Adam Coates, Andrew Y Ng, and Honglak Lee. An analysis of single-layer networks in unsupervised feature learning. *Proceedings of the fourteenth International Conference on Artificial Intelligence and Statistics*, pages 215–223, 2011.
- [15] Corinna Cortes, Mehryar Mohri, and Afshin Rostamizadeh. Algorithms for learning kernels based on centered alignment. *The Journal of Machine Learning Research*, 13(1):795–828, 2012.
- [16] Jia Deng, Wei Dong, Richard Socher, Li-Jia Li, Kai Li, and Li Fei-Fei. Imagenet: A large-scale hierarchical image database. *2009 IEEE Conference on Computer Vision and Pattern Recognition*, pages 248–255, 2009.
- [17] Jacob Devlin, Ming-Wei Chang, Kenton Lee, and Kristina Toutanova. Bert: Pre-training of deep bidirectional transformers for language understanding. *arXiv preprint arXiv:1810.04805*, 2018.
- [18] Jeff Donahue, Yangqing Jia, Oriol Vinyals, Judy Hoffman, Ning Zhang, Eric Tzeng, and Trevor Darrell. Decaf: A deep convolutional activation feature for generic visual recognition. In *International Conference on Machine Learning*, pages 647–655. PMLR, 2014.
- [19] Clément Farabet, Camille Couprie, Laurent Najman, and Yann LeCun. Learning hierarchical features for scene labeling. *IEEE Transactions on Pattern Analysis and Machine Intelligence*, 35(8):1915–1929, 2013.
- [20] Li Fei-Fei, Rob Fergus, and Pietro Perona. Learning generative visual models from few training examples: an incremental bayesian approach tested on 101 object categories. In *2007 IEEE Conference on Computer Vision and Pattern Recognition*, pages 1–8, 2007.
- [21] Ian Goodfellow, Yoshua Bengio, and Aaron Courville. *Deep learning*. MIT press, 2016.
- [22] Kaiming He, Xiangyu Zhang, Shaoqing Ren, and Jian Sun. Deep residual learning for image recognition. *Proceedings of the IEEE Conference on Computer Vision and Pattern Recognition*, 2016.
- [23] Gao Huang, Danlu Chen, Tianhong Li, Felix Wu, Laurens Van Der Maaten, and Kilian Q Weinberger. Multi-scale dense networks for resource efficient image classification. In *International Conference on Learning Representations*, 2018.
- [24] Gao Huang, Zhuang Liu, Laurens van der Maaten, and Kilian Q Weinberger. Densely connected convolutional networks. *Proceedings of the IEEE Conference on Computer Vision and Pattern Recognition*, pages 4700–4708, 2017.
- [25] Shuqiang Jiang, Weiqing Min, Linhu Liu, and Zhengdong Luo. Multi-scale multi-view deep feature aggregation for food recognition. *IEEE Transactions on Image Processing*, 29:265–276, 2020.
- [26] Licheng Jiao, Jie Gao, Xu Liu, Fang Liu, Shuyuan Yang, and Biao Hou. Multiscale representation learning for image classification: A survey. *IEEE Transactions on Artificial Intelligence*, 4(1):23–43, 2023.
- [27] Simon Kornblith, Mohammad Norouzi, Honglak Lee, and Geoffrey Hinton. Similarity of neural network representations revisited. In *International Conference on Machine Learning*, pages 3519–3529. PMLR, 2019.
- [28] Jonathan Krause, Michael Stark, Jia Deng, and Li Fei-Fei. 3d object representations for fine-grained categorization. In *4th International IEEE Workshop on 3D Representation and Recognition (3dRR-13)*. IEEE, 2013.
- [29] Alex Krizhevsky, Geoffrey Hinton, et al. Learning multiple layers of features from tiny images. 2009.
- [30] Alex Krizhevsky, Ilya Sutskever, and Geoffrey E Hinton. Imagenet classification with deep convolutional neural networks. *Advances in Neural Information Processing Systems*, pages 1097–1105, 2012.
- [31] Yann LeCun, Yoshua Bengio, and Geoffrey Hinton. Deep learning. *Nature*, 521(7553):436–444, 2015.

- [32] Stefan Leutenegger, Margarita Chli, and Roland Y Siegwart. Brisk: Binary robust invariant scalable keypoints. In *2011 International Conference on Computer Vision*, pages 2548–2555. IEEE, 2011.
- [33] Shan Li, Weihong Deng, and JunPing Du. Reliable crowdsourcing and deep locality-preserving learning for expression recognition in the wild. In *Proceedings of the IEEE Conference on Computer Vision and Pattern Recognition*, pages 2852–2861, 2017.
- [34] Tsung-Yi Lin, Piotr Dollár, Ross Girshick, Kaiming He, Bharath Hariharan, and Serge Belongie. Feature pyramid networks for object detection. In *Proceedings of the IEEE Conference on Computer Vision and Pattern Recognition*, pages 2117–2125, 2017.
- [35] Shu Liu, Xiaojuan Qi, Jianping Shi, Hong Zhang, and Jiaya Jia. Multi-scale patch aggregation (mpa) for simultaneous detection and segmentation. In *Proceedings of the IEEE Conference on Computer Vision and Pattern Recognition*, pages 3141–3149, 2016.
- [36] David G Lowe. Distinctive image features from scale-invariant keypoints. volume 60, pages 91–110. Springer, 2004.
- [37] Subhansu Maji, Esa Rahtu, Juho Kannala, Matthew Blaschko, and Andrea Vedaldi. Fine-grained visual classification of aircraft. 2013.
- [38] Jiri Matas, Ondrej Chum, Martin Urban, and Tomás Pajdla. Robust wide-baseline stereo from maximally stable extremal regions. *Image and Vision Computing*, 22(10):761–767, 2004.
- [39] Jean-Michel Morel and Guoshen Yu. Asift: A new framework for fully affine invariant image comparison. *SIAM Journal on Imaging Sciences*, 2(2):438–469, 2009.
- [40] Lichao Mou, Yuansheng Hua, and Xiao Xiang Zhu. Relation matters: Relational context-aware fully convolutional network for semantic segmentation of high-resolution aerial images. *IEEE Transactions on Geoscience and Remote Sensing*, 58(11):7557–7569, 2020.
- [41] Maria-Elena Nilsback and Andrew Zisserman. Automated flower classification over a large number of classes. *Proceedings of the Indian Conference on Computer Vision, Graphics and Image Processing*, pages 722–729, 2008.
- [42] Vardan Papyan and Michael Elad. Multi-scale patch-based image restoration. *IEEE Transactions on Image Processing*, 25(1):249–261, 2016.
- [43] Omkar M Parkhi, Andrea Vedaldi, Andrew Zisserman, and CV Jawahar. Cats and dogs. In *2012 IEEE Conference on Computer Vision and Pattern Recognition*, pages 3498–3505. IEEE, 2012.
- [44] Siyuan Qiao, Zhishuai Zhang, Wei Shen, Bo Wang, and Alan Yuille. Gradually updated neural networks for large-scale image recognition. *International Conference on Machine Learning*, pages 4188–4197, 2018.
- [45] Alec Radford, Karthik Narasimhan, Tim Salimans, and Ilya Sutskever. Improving language understanding by generative pre-training. *OpenAI Blog*, 1(8), 2018.
- [46] Mark Sandler, Andrew Howard, Menglong Zhu, Andrey Zhmoginov, and Liang-Chieh Chen. Mobilenetv2: Inverted residuals and linear bottlenecks. In *Proceedings of the IEEE Conference on Computer Vision and Pattern Recognition*, pages 4510–4520, 2018.
- [47] Jun Shi, Yanan Zhao, Wei Xiang, Vishal Monga, Xiaoping Liu, and Ran Tao. Deep scattering network with fractional wavelet transform. *IEEE Transactions on Signal Processing*, 69:4740–4757, 2021.
- [48] Bing Shuai, Zhen Zuo, Bing Wang, and Gang Wang. Scene segmentation with dag-recurrent neural networks. *IEEE Transactions on Pattern Analysis and Machine Intelligence*, 40(6):1480–1493, 2018.
- [49] Karen Simonyan, Andrea Vedaldi, and Andrew Zisserman. Deep inside convolutional networks: Visualising image classification models and saliency maps. *arXiv preprint arXiv:1312.6034*, 2013.
- [50] Karen Simonyan and Andrew Zisserman. Very deep convolutional networks for large-scale image recognition. *arXiv preprint arXiv:1409.1556*, 2014.
- [51] Jost Tobias Springenberg, Alexey Dosovitskiy, Thomas Brox, and Martin Riedmiller. Striving for simplicity: The all convolutional net. 2014.
- [52] Ilya Sutskever, Oriol Vinyals, and Quoc V Le. Sequence to sequence learning with neural networks. *Advances in Neural Information Processing Systems*, pages 3104–3112, 2014.
- [53] Christian Szegedy, Wei Liu, Yangqing Jia, Pierre Sermanet, Scott Reed, Dragomir Anguelov, Dumitru Erhan, Vincent Vanhoucke, and Andrew Rabinovich. Going deeper with convolutions. *Proceedings of the IEEE Conference on Computer Vision and Pattern Recognition*, pages 1–9, 2015.
- [54] Christian Szegedy, Vincent Vanhoucke, Sergey Ioffe, Jon Shlens, and Zbigniew Wojna. Rethinking the inception architecture for computer vision. *Proceedings of the IEEE Conference on Computer Vision and Pattern Recognition*, pages 2818–2826, 2016.
- [55] Hossein Talebi and Peyman Milanfar. Learning to resize images for computer vision tasks. *Proceedings of the IEEE/CVF International Conference on Computer Vision*, pages 497–506, 2021.
- [56] Hugo Touvron, Andrea Vedaldi, Matthijs Douze, and Hervé Jégou. Fixing the train-test resolution discrepancy. *Advances in Neural Information Processing Systems*, 2019.
- [57] Ashish Vaswani, Noam Shazeer, Niki Parmar, Jakob Uszkoreit, Llion Jones, Aidan N Gomez, Lukasz Kaiser, and Illia Polosukhin. Attention is all you need. In *Advances in Neural Information Processing Systems*, pages 5998–6008, 2017.
- [58] Rosaura G VidalMata, Sreya Banerjee, Brandon RichardWebster, Michael Albright, Pedro Davalos, Scott McCloskey, Ben Miller, Asong Tambo, Sushobhan Ghosh, Sudarshan Nagesh, et al. Bridging the gap between computational photography and visual recognition. *IEEE transactions on pattern analysis and machine intelligence*, 43(12):4272–4290, 2020.
- [59] Jingdong Wang, Ke Sun, Tianheng Cheng, Borui Jiang, Chaorui Deng, Yang Zhao, Dong Liu, Yadong Mu, Minghui Tan, Xinggang Wang, Wenyu Liu, and Bin Xiao. Deep high-resolution representation learning for visual recognition. *IEEE Transactions on Pattern Analysis and Machine Intelligence*, 43(10):3349–3364, 2021.
- [60] Xin Wang, Fisher Yu, Ziwei Liang, Thomas Huang, Larry Shi, Matthew Liu, Jan Kautz, and Alan Yuille. Resolution adaptive networks for efficient inference. *Proceedings of the IEEE/CVF Conference on Computer Vision and Pattern Recognition*, pages 8729–8738, 2018.
- [61] Thomas Wiatowski and Helmut Bölcskei. A mathematical theory of deep convolutional neural networks for feature extraction. *IEEE Transactions on Information Theory*, 64(3):1845–1866, 2018.
- [62] Fangting Xia, Peng Wang, Liang-Chieh Chen, and Alan L Yuille. Zoom better to see clearer: Human part segmentation with auto zoom net. In *Proc. of the European Conference on Computer Vision (ECCV)*, volume 1. Citeseer, 2016.
- [63] Han Xiao, Kashif Rasul, and Roland Vollgraf. Fashion-mnist: a novel image dataset for benchmarking machine learning algorithms. *arXiv preprint arXiv:1708.07747*, 2017.
- [64] Saining Xie, Ross Girshick, Piotr Dollár, Zhuowen Tu, and Kaiming He. Aggregated residual transformations for deep neural networks. In *Proceedings of the IEEE Conference on Computer Vision and Pattern Recognition*, pages 1492–1500, 2017.
- [65] Yichong Xu, Tianjun Xiao, Jiaying Zhang, Kuiyuan Yang, and Zheng Zhang. Scale-invariant convolutional neural networks. *arXiv preprint arXiv:1411.6369*, 2014.
- [66] Wenfei Yang, Tianzhu Zhang, Zhendong Mao, Yongdong Zhang, Qi Tian, and Feng Wu. Multi-scale structure-aware network for weakly supervised temporal action detection. *IEEE Transactions on Image Processing*, 30:5848–5861, 2021.
- [67] Xin Yang and Kwang-Ting Tim Cheng. Local difference binary for ultrafast and distinctive feature description. *IEEE Transactions on Pattern Analysis and Machine Intelligence*, 36(1):188–194, 2014.
- [68] Jason Yosinski, Jeff Clune, Yoshua Bengio, and Hod Lipson. How transferable are features in deep neural networks? *Advances in Neural Information Processing Systems*, 2014.
- [69] Jun Yu, Min Tan, Hongyuan Zhang, Yong Rui, and Dacheng Tao. Hierarchical deep click feature prediction for fine-grained image recognition. *IEEE Transactions on Pattern Analysis and Machine Intelligence*, 44(2):563–578, 2022.
- [70] Jun Yu, Chaoyang Zhu, Jian Zhang, Qingming Huang, and Dacheng Tao. Spatial pyramid-enhanced netvlad with weighted triplet loss for place recognition. *IEEE Transactions on Neural Networks and Learning Systems*, 31(2):661–674, 2020.
- [71] Matthew D Zeiler and Rob Fergus. Visualizing and understanding convolutional networks. In *Computer Vision—ECCV 2014: 13th European Conference, Zurich, Switzerland, September 6–12, 2014, Proceedings, Part I 13*, pages 818–833. Springer, 2014.
- [72] Hengshuang Zhao, Jianping Shi, Xiaojuan Qi, Xinggang Wang, and Jiaya Jia. Pyramid scene parsing network. In *Proceedings of the IEEE Conference on Computer Vision and Pattern Recognition*, pages 2881–2890, 2017.
- [73] Zengqun Zhao, Qingshan Liu, and Shanmin Wang. Learning deep global multi-scale and local attention features for facial expression recognition in the wild. *IEEE Transactions on Image Processing*, 30:6544–6556, 2021.
- [74] Yongxiang Zou and Long Cheng. A transfer learning model for gesture recognition based on the deep features extracted by cnn. *IEEE Transactions on Artificial Intelligence*, 2(5):447–458, 2021.